Intermetallics 107 (2019) 34–38

Contents lists available at ScienceDirect

Intermetallics

journal homepage: www.elsevier.com/locate/intermet

Dilatancy signatures of amorphous plasticity probed by X-ray synchrotron radiation

X. Sun[a,b], G. Ding[a,c], G. Mo[d], L.H. Dai[a,b], M.Q. Jiang[a,b,*]

[a] State Key Laboratory of Nonlinear Mechanics, Institute of Mechanics, Chinese Academy of Sciences, Beijing, 100190, People's Republic of China
[b] School of Engineering Science, University of Chinese Academy of Sciences, Beijing, 100049, People's Republic of China
[c] State Key Laboratory for Mechanical Behavior of Materials, Xi'an Jiaotong University, Xi'an, 710049, People's Republic of China
[d] Synchrotron Radiation Laboratory, Institute of High Energy Physics, Chinese Academy of Sciences, Beijing 100039, People's Republic of China

ARTICLE INFO

Keywords:
Amorphous alloys
Plastic deformation
X-ray synchrotron radiation
Dilatancy
Shear transformations

ABSTRACT

The dilatancy signatures associated with the plastic deformation of a typical Zr-based amorphous alloy are captured by using synchrotron radiation X-ray diffraction (XRD) and small angle X-ray scattering (SAXS) techniques. XRD demonstrates that the right-subpeak atoms of the second coordination shell accommodate the local dilatation, which occurs prior to the plastic yielding and during the softening-to-flow transition process. Mediated by the local dilatation, local atomic rearrangements can operate at the left-subpeak of the second shell and/or at the fourth shell with a characteristic lengthscale of about 1 nm. The obtained dilatancy signatures of amorphous plasticity are further confirmed by SAXS in terms of the nano-scale structural heterogeneity.

1. Introduction

The long-range atomic disorder in amorphous alloys poses a great challenge for understanding their flow mechanism within a consistent physical framework [1–7]. Defects underpinning plastic flow in their crystalline cousins, such as dislocations or grain boundaries, are not present. Instead, amorphous plasticity is attributed to local irreversible rearrangements of atomic groups, originally defined as "shear transformations (STs)" by Argon [2]. It is well accepted that one of fundamental properties of STs is the dilatancy [7–10]. Specifically, the occurrence of STs is always accompanied with the generation of local free volume. In addition to stress and temperature, the local dilatation provides a configurational driving-force for the activation of STs [6,8,11,12]. Actually, the inherent competition between shear and dilatation during STs determines almost all mechanical behaviors, including yielding and flow [13,14], shear-banding [10,15] and its-induced cracking [16,17], ductile-brittle transition in fracture [18–20], ect. Despite of its significance, how to quantitatively detect the dilatancy of STs remains a challenge especially from an experimental view.

Synchrotron radiation X-ray diffraction (XRD) provides a feasible way to probe short-range-order (SRO) to medium-range-order (MRO) structural evolution during the deformation of materials [21,22]. Atomic level strains can be extracted from the diffraction data or the pair distribution function (PDF). For amorphous alloys lacking ordered lattices, the atomic strains are usually lengthscale-dependent in response to applied macroscopic deformation [23–25]. This trans-scale mismatch of deformation stems from the difference of local environments where atoms reside in, which sheds insight into the structural responses of amorphous plasticity. For example, by decomposing the atomic strains at different coordination shells as a function of macroscopic stress or strain, the dominated shell accommodating local deformation can be determined at MRO [26–28]. Wang et al. [29] proposed a nano-scale concordant region to bridge the bond-exchange at SRO and the macroscopic yielding. These reports indicate the existence of nano-scale local soft regions where STs occur preferably. However, what structure is responsible for STs' dilatancy is still unknown and deserves further investigations.

On the other hand, ST operations will in turn redistribute local soft regions and remaining strongly bonded domains (local hard regions) [30–32]. Therefore, a direct nano-scale structural probe into amorphous deformation is necessary. Synchrotron radiation small angle X-ray scattering (SAXS) provides such a possibility [33–36], by measuring the fluctuation of local electronic density to reflect nano-scale packing heterogeneity. Recently, Sun et al. [37] performed an in situ SAXS during uniaxial tension of a Vitreloy 1 amorphous alloy, and detected nano-scale scatterers with a complex spatial distribution. Nevertheless, they did not focus on the dilatancy of deformation from the SAXS signatures.

* Corresponding author. State Key Laboratory of Nonlinear Mechanics, Institute of Mechanics, Chinese Academy of Sciences, Beisihuanxi Road 15, Beijing, 100190, China.
E-mail address: mqjiang@imech.ac.cn (M.Q. Jiang).

https://doi.org/10.1016/j.intermet.2019.01.009
Received 3 November 2018; Received in revised form 6 December 2018; Accepted 6 January 2019

In this paper, we conduct ex situ synchrotron radiation XRD and SAXS measurements of a typical Zr-based amorphous alloy that is frozen at different stages of compressive deformation. The dilatancy of the plastic deformation is clearly detected, and its role during the flow event (ST) is discussed as well.

2. Experiments

The bulk amorphous alloy (Vitreloy 105), with the nominal composition of $Zr_{52.5}Ti_5Cu_{17.9}Ni_{14.6}Al_{10}$ (at. %), was prepared by suck casting from master alloys ingots to a water-cooled copper mould in an arc furnace. Uniaxial compressions were performed on rod-shaped samples (Φ5 mm × 10 mm) with an Instron 8852 type machine under a strain rate of $6 \times 10^{-3}\,s^{-1}$ at a temperature of 643 K (35 K below the glass transition temperature T_g). Before loading, 1 h heat-preservation at 643 K was applied on the sample to eliminate the relaxation effects. Under the chosen conditions, all samples undergo a homogenous deformation without shear bands. A series of samples were compressed to different total strains followed by unload and rapid quenching into iced water. We then obtained six transient configurations of the deformation ranging from elastic, plastic yielding to flow stages. The inelastic strain (total strain minus elastic strain [38]) for each configuration was measured using a micrometer caliper with an accuracy of ± 5 μm. After that, thin slices perpendicular to the loading axis were cut from each configuration by diamond saw blade and then carefully polished to 1 mm thick for XRD and 0.02 mm thick for SAXS. The XRD and SAXS measurements were carried out respectively at 4B9A and 1W2A beam lines of the Beijing synchrotron radiation facility (BSRF) [39].

3. Results and discussion

Fig. 1 presents typical stress-strain curves of the samples compressed to total uniaxial stains ranging from 0.015 to 0.090. For the six transient configurations, their inelastic strains are 0.0018, 0.0082, 0.0218, 0.0327, 0.0545 and 0.0751, respectively. These transient configurations capture typical deformation stages including: (a) and (b) apparently elastic deformation, (c) macroscopic plastic yielding with a typical stress overshoot, (d) and (e) strain softening or stress drop, and (f) onset of homogeneous flow. The observed constitutive behaviors can be well explained in terms of the interaction of STs and free volume (local dilatation) dynamics [6]. It is noteworthy that the plastic yielding occurs at an inelastic strain of 0.0218. This critical strain obeys the $T^{2/3}$ scaling law reported by Johnson and Samwer [4] based on the

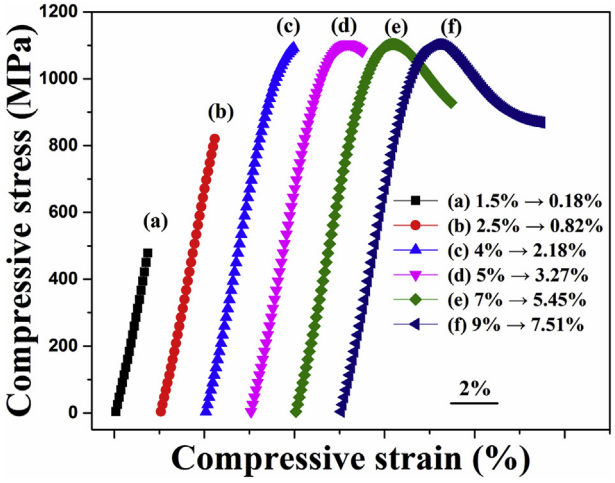

Fig. 1. The stress–strain curves of the Vitreloy 105 amorphous alloy at 643 K compressed to different total strains: (a) 0.015, (b) 0.025, (c) 0.040, (d) 0.050, (e) 0.070, and (f) 0.090. The corresponding inelastic strains are (a) 0.0018, (b) 0.0082, (c) 0.0218, (d) 0.0327, (e) 0.0545, and (f) 0.0751.

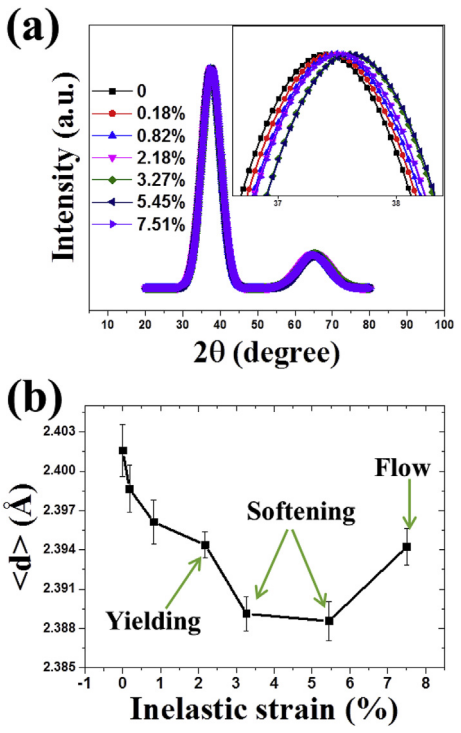

Fig. 2. (a) XRD intensity curves of the Vitreloy 105 amorphous alloy at different inelastic strains; Inset highlights the positions of the first peaks. (b) Change of the average interatomic distance with the inelastic strain.

cooperative shear of STs.

Fig. 2(a) gives the XRD intensity curves of the six transient configurations and the unstrained as-cast state, and the first diffraction peaks are enlarged in the inset. The average interatomic distance $\langle d \rangle$ can be calculated by the position of the first peak according to Bragg's law, which varies with the inelastic strain, as shown in Fig. 2 (b). According to the work reported by Huang et al. [40], the weakest solvent-solvent (Zr−Zr) atomic pair should make a dominated contribution to change of the $\langle d \rangle$. Under the macroscopic compression, the $\langle d \rangle$ decreases monotonically even after the plastic yielding. However, with the occurrence of strain softening, the decrease of $\langle d \rangle$ slows down, and eventually turns to increase during the softening-to-flow (STF) transition process. It is also noted that there is a decrease retardance of $\langle d \rangle$ at the inelastic strain of 0.0218 when the plastic yielding occurs. These results clearly indicate that the dilatation of atomic packing is closely associated with the plastic yielding or flow, which compensates or even overcomes the decrease of $\langle d \rangle$ induce by the macroscopic compression.

We further study the dilatancy effect of plasticity in real space to ferret out its structural origin. Fig. 3(a) shows the PDFs by taking the Fourier transform of the XRD intensity curves in Fig. 2(a). The PDF describes the average probability for finding atoms at a distance r from a given atom [25,28]. From the PDF curves, we identify a series of peaks corresponding to the first six coordination shells that cover the lengthscale ranging from SRO to MRO. One can notice that all of the second peaks split into two subpeaks (right and left), which represents a typical glass structure [41]. Based on these coordination peaks in PDF, we shall define the local atomic strain as [42,43] $\varepsilon_l = (r_p - r_p^0)/r_p^0$, p=1, 2-1, 2-2, 3, 4, 5, and 6, where r_p^0 and r_p denote the peak positions before and after compression, respectively. The ε_l measures the relative change of average position of atoms in different shells due to the macroscopic compression. Fig. 3(b) presents the distribution of the local atomic strains ε_l along different coordination shells, which evolves with the macroscopic inelastic strains. Overall, the distribution of ε_l is spatially heterogeneous upon the deformation. Compared to other reports [26–28], an intriguing finding is that the right subpeak r_{2-2} of the

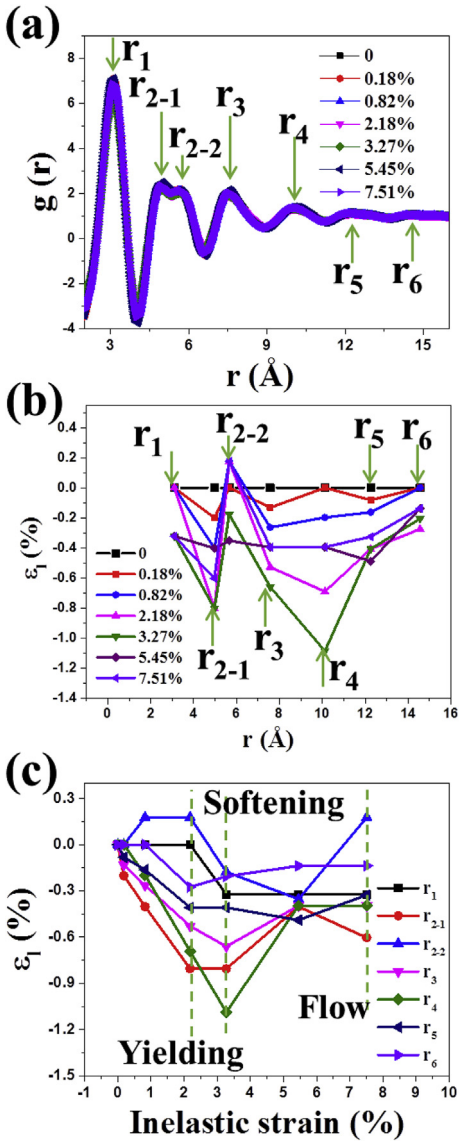

Fig. 3. (a) Pair distribution functions at different inelastic strains. (b) Distribution of local atomic strains at different coordination shells with increasing inelastic strains. (c) Local atomic strains as a function of inelastic strains at different coordination shells.

second shell undergoes abnormal tensile strains during certain deformation stages. To make this clearer, we plot the local atomic strain ε_l as a function of the inelastic strain at different coordination shells, as shown in Fig. 3(c). Obviously, the abnormal tension at r_{2-2} only occurs before the macroscopic yielding and during the STF transition process. This is consistent with the dilatation signatures denoted by the $\langle d \rangle$ in Fig. 2(b), demonstrating the structural origin of the plasticity dilatancy. Importantly, the characteristic lengthscale of the local dilatation is of about 0.56 nm at r_{2-2}, not at the usually suggested single-atomic-scale [1]. This agrees well with the finding reported by Lu et al. [7] who used a colloidal glass to simulate amorphous plasticity. They found that local free volume or dilatation that shows the best correction with STs should be coarse-grained to a lengthscale near the second shell. The agreement suggests that amorphous alloys and colloidal glasses share the identical mechanisms of plasticity [5,44], although their constituent particles have a huge size-difference of at least 4 orders of magnitude.

It is further noted that local compressive strains are accommodated mainly by the left subpeak at r_{2-1} and the fourth shell at r_4, leading to two peaks in Fig. 3(b). Before the macroscopic yielding, the former is even stronger than the latter. This implies that the plasticity is triggered by rearrangements of the second-shell atoms. A reasonable reason is that the second shell simultaneously accommodates the local dilatation before the plastic yielding. However, the r_{2-1} subpeak does not contribute any longer to subsequent strain softening that is mainly dominated by the r_4 shell. We find that the fourth shell is at the lengthscale of about 1 nm, which is the characteristic size of local atomic cluster accommodating the largest local strain. Similar results were also reported for compression [23,26] or tension [25,27] of other amorphous alloys, in which local atomic strain shows a peak at the lengthscale around 1 nm. These lenghscales are consistent with the characteristic sizes of STs [45,46], identifying STs as basic carriers of amorphous plasticity. At last, it seems that the second shell is responsible again for the homogeneous flow where local tensile and compressive strains rebuild at the r_{2-2} and r_{2-1} subpeaks, respectively.

The above analyses point to a fundamental flow event for amorphous plasticity. When an external deformation is applied, all coordination shells make responses immediately to accommodate local strains except the first one. Due to inherent fluctuations of coordination atoms [41], the second shell participates preferentially in deformation at its left subpeak, and simultaneously accommodates the deformation-induced dilatation at its right subpeak. The positive interplay between deformation and dilatation [6] triggers STs at the second shell. In fact, by simulating the activation processes in a metallic glass model, Fan et al. [47] also found that thermally activated deformation originates from subnano-scale rearrangements of a small number of atoms. At the same time, the ST can spatially extend to the fourth shell at the lengthscale of about 1 nm. The two-shell cooperative rearrangements during STs lead to macroscopically perceptible plastic yielding. However, the subsequent strain softening is mainly attributed to the fourth-shell rearrangements at larger lengthscales. With the onset of homogeneous flow, the second-shell rearrangements at smaller lengthscales dominate the deformation and dilatation again. It is believed that the transfer of atomic rearrangements between r_{2-1} and r_4 is mediated by the local dilatation at r_{2-2}. The change of characteristic size of STs during different deformation stages was also proposed by Shao et al. [48] based on the high-resolution observations of shear bands and by Jiang et al. [10] to theoretically predict local dilatation in shear bands. Our present result confirms their proposal, all showing that the characteristic size of STs at the mature flow stage is relatively smaller than that at the initial deformation stage.

Finally, we examine the STs' dilatancy by SAXS at the nanoscale structural level, which is not touched upon previously. Fig. 4(a) presents the SAXS intensity $I(q)$ curves for the six deformed configurations and the unstrained as-cast state, and the inset shows that there is indeed a slight variation of $I(q)$ with the inelastic strain. To get a quantitative result, we calculate the SAXS integral invariant [49] $Q = \int_0^\infty I(q)q^2 \mathrm{d}q$, which measures the average fluctuation of nano-scale scatters that are local soft and hard regions of atoms here [37]. Fig. 4(b) shows the integral invariant Q as a function of the inelastic strain. Very interestingly, the variation trend of Q is totally identical with that of the average interatomic distance $\langle d \rangle$ in Fig. 2(b), and certainly the directions are opposite. The consistence implies that the local dilatation at r_{2-2} can be perceived not only in terms of the $\langle d \rangle$ at the atomic-scale, but also by the nano-scale structural heterogeneity. It is well known that an amorphous structure consists of nano-scale local soft and hard regions [50–52]. Clearly, the pure elastic compression could strengthen the interface of two regions, corresponding to an increase of the Q. However, ST operations with local dilatation in soft regions will lead to the collapse of surrounding hard regions, which blurs or weakens the interface between hard and soft regions. Therefore, the ST's dilatancy is responsible for the slowing down of the Q increase at the plastic yielding, and the decrease of the Q during the STF transition process.

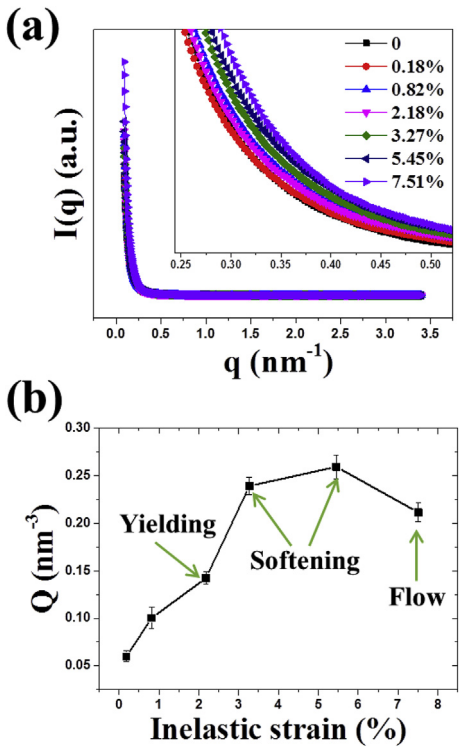

Fig. 4. (a) Small angel X-ray scattering intensity curves of the Vitreloy 105 amorphous alloy at different inelastic strains; Inset highlights the change of the curves. (b) Integral invariant of scattering intensity as a function of inelastic strains.

4. Conclusions

In summary, this study provides compelling evidence for the dilatancy of amorphous plasticity. We use the X-ray synchrotron radiation to probe the atomic-to-nano-scale structural evolution of a typical amorphous alloy frozen at different deformation stages. It is revealed that local dilatation is accommodated by the second coordination shell, which operates before the plastic yielding and during the STF transition process. The subnano-scale local dilatation can mediate the transfer of atomic rearrangements between the second and fourth coordination shells, identifying a nano-scale flow event as ST. Finally, the dilatancy of amorphous plasticity can be indicated by the nano-scale structural heterogeneity. These findings shed new insight into the dilatancy of STs and further improve the ST picture of amorphous plasticity. In the present work, both macroscopic deformation and atomic strains are discussed from a sample-averaged perspective. However, once we further consider the spatial heterogeneity of ST's dilatancy [7], the localization of plastic flow into shear bands can be understood [15,53,54]. The picture from ST-mediated dilatation (or local free volume) to amorphous shear banding has been extensively described in Refs. [10,55].

Acknowledgments

This work was supported by the National Natural Science Foundation of China (Grant Nos. 11522221 and 11790292), the Strategic Priority Research Program (Grant No. XDB22040303), and the Key Research Program of Frontier Sciences (Grant No. QYZDJSSW-JSC011) of the Chinese Academy of Sciences.

References

[1] F. Spaepen, A microscopic mechanism for steady state inhomogeneous flow in metallic glasses, Acta Metall. 25 (1977) 407–415.
[2] A.S. Argon, Plastic deformation in metallic glasses, Acta Metall. 27 (1979) 47–58.
[3] M.L. Falk, J.S. Langer, Dynamics of viscoplastic deformation in amorphous solids, Phys. Rev. E 57 (1998) 7192–7205.
[4] W.L. Johnson, K. Samwer, A universal criterion for Plastic yielding of metallic glasses with a $(T/T_g)^{2/3}$ temperature dependence, Phys. Rev. Lett. 95 (2005) 195501.
[5] P. Schall, D.A. Weitz, F. Spaepen, Structural rearrangements that govern flow in colloidal glasses, Science 318 (2007) 1895–1899.
[6] M.Q. Jiang, G. Wilde, L.H. Dai, Origin of stress overshoot in amorphous solids, Mech. Mater. 81 (2015) 72–83.
[7] Y.Z. Lu, M.Q. Jiang, X. Lu, Z.X. Qin, Y.J. Huang, J. Shen, Dilatancy of shear transformations in a colloidal glass, Phys. Rev. Applied 9 (2018) 014023.
[8] A. Lemaître, Rearrangements and dilatancy for dheared dense materials, Phys. Rev. Lett. 89 (2002) 195503.
[9] Y.J. Wang, M.Q. Jiang, Z.L. Tian, L.H. Dai, Direct atomic-scale evidence for shear-dilatation correlation in metallic glasses, Scripta Mater. 112 (2016) 37–41.
[10] M.Q. Jiang, G. Wilde, L.H. Dai, Shear band dilatation in amorphous alloys, Scripta Mater. 127 (2017) 54–57.
[11] J.S. Langer, Dynamics of shear-transformation zones in amorphous plasticity: formulation in terms of an effective disorder temperature, Phys. Rev. E 70 (2004) 041502.
[12] L. Li, E.R. Homer, C.A. Schuh, Shear transformation zone dynamics model for metallic glasses incorporating free volume as a state variable, Acta Mater. 61 (2013) 3347–3359.
[13] L. Sun, M.Q. Jiang, L.H. Dai, Intrinsic correlation between dilatation and pressure sensitivity of plastic flow in metallic glasses, Scripta Mater. 63 (2010) 943–946.
[14] C.A. Schuh, A.C. Lund, Atomistic basis for the plastic yield criterion of metallic glass, Nat. Mater. 2 (2003) 449–452.
[15] M.Q. Jiang, L.H. Dai, On the origin of shear banding instability in metallic glasses, J. Mech. Phys. Solid. 57 (2009) 1267–1292.
[16] P. Murali, R. Narasimhan, T.F. Guo, Y.W. Zhang, H.J. Gao, Shear bands mediate cavitation in brittle metallic glasses, Scripta Mater. 68 (2013) 567–570.
[17] F. Zeng, M.Q. Jiang, L.H. Dai, Dilatancy induced ductile-brittle transition of shear band in metallic glasses, Proc. Roy. Soc. Lond. A 474 (2018) 20170836.
[18] M.Q. Jiang, Z. Ling, J.X. Meng, L.H. Dai, Energy dissipation in fracture of bulk metallic glasses via inherent competition between local softening and quasi-cleavage, Philos. Mag. A 88 (2008) 407–426.
[19] R. Raghavan, P. Murali, U. Ramamurty, On factors influencing the ductile-to-brittle transition in a bulk metallic glass, Acta Mater. 57 (2009) 3332–3340.
[20] M.Q. Jiang, G. Wilde, J.H. Chen, C.B. Qu, S.Y. Fu, F. Jiang, L.H. Dai, Cryogenic-temperature-induced transition from shear to dilatational failure in metallic glasses, Acta Mater. 77 (2014) 248–257.
[21] M. Stoica, J. Das, J. Bednarcik, H. Franz, N. Mattern, W.H. Wang, J. Eckert, Strain distribution in Zr64.13Cu15.75Ni10.12Al10 bulk metallic glass investigated by in situ tensile tests under synchrotron radiation, J. Appl. Phys. 104 (2008) 013522.
[22] M. Stoica, J. Das, J. Bednarčik, G. Wang, G. Vaughan, W.H. Wang, J. Eckert, Mechanical response of metallic glasses: insights from in-situ high energy X-ray diffraction, JOM 62 (2010) 76–82.
[23] H.F. Poulsen, J.A. Wert, J. Neuefeind, V. Honkimaki, M. Daymond, Measuring strain distributions in amorphous materials, Nat. Mater. 4 (2005) 33–36.
[24] J. Das, M. Boström, N. Mattern, Å. Kvick, A.R. Yavari, A.L. Greer, J. Eckert, Plasticity in bulk metallic glasses investigated via the strain distribution, Phys. Rev. B 76 (2007) 092203.
[25] X.D. Wang, J. Bednarcik, H. Franz, H.B. Lou, Z.H. He, Q.P. Cao, J.Z. Jiang, Local strain behavior of bulk metallic glasses under tension studied by in situ x-ray diffraction, Appl. Phys. Lett. 94 (2009) 011911.
[26] T.C. Hufnagel, R.T. Ott, J. Almer, Structural aspects of elastic deformation of a metallic glass, Phys. Rev. B 73 (2006) 064204.
[27] X.D. Wang, J. Bednarcik, K. Saksl, H. Franz, Q.P. Cao, J.Z. Jiang, Tensile behavior of bulk metallic glasses by in situ x-ray diffraction, Appl. Phys. Lett. 91 (2007) 081913.
[28] H. Shakur Shahabi, S. Scudino, I. Kaban, M. Stoica, U. Rütt, U. Kühn, J. Eckert, Structural aspects of elasto-plastic deformation of a Zr-based bulk metallic glass under uniaxial compression, Acta Mater. 95 (2015) 30–36.
[29] G. Wang, N. Mattern, J. Bednarčík, R. Li, B. Zhang, J. Eckert, Correlation between elastic structural behavior and yield strength of metallic glasses, Acta Mater. 60 (2012) 3074–3083.
[30] E.D. Cubuk, R.J.S. Ivancic, S.S. Schoenholz, D.J. Strickland, A. Basu, Z.S. Davidson, J. Fontaine, J.L. Hor, Y.R. Huang, Y. Jiang, N.C. Keim, K.D. Koshigan, J.A. Lefever, T. Liu, X.G. Ma, D.J. Magagnosc, E. Morrow, C.P. Ortiz, J.M. Rieser, A. Shavit, T. Still, Y. Xu, Y. Zhang, K.N. Nordstrom, P.E. Arratia, R.W. Carpick, D.J. Durian, Z. Fakhraai, D.J. Jerolmack, D. Lee, J. Li, R. Riggleman, K.T. Turner, A.G. Yodh, D.S. Gianola, A.J. Liu, Structure-property relationships from universal signatures of plasticity in disordered solids, Science 358 (2017) 1033–1037.
[31] Z. Wang, P. Wen, L.S. Huo, H.Y. Bai, W.H. Wang, Signature of viscous flow units in apparent elastic regime of metallic glasses, Appl. Phys. Lett. 101 (2012) 121906.
[32] M.L. Manning, A.J. Liu, Vibrational modes identify soft spots in a sheared disordered packing, Phys. Rev. Lett. 107 (2011) 108302.
[33] X.L. Wang, J. Almer, C.T. Liu, Y.D. Wang, J.K. Zhao, A.D. Stoica, D.R. Haeffner, W.H. Wang, In situ synchrotron study of phase transformation behaviors in bulk metallic glass by simultaneous diffraction and small angle scattering, Phys. Rev. Lett. 91 (2003) 265501.
[34] M. Zhang, L.H. Dai, Y. Liu, L. Liu, Heterogeneous dynamics of metallic glasses, Scripta Mater. 107 (2015) 111–114.
[35] X.J. Liu, X.D. Hui, G.L. Chen, M.H. Sun, In situ synchrotron SAXS study of nanocrystallization in Zr65Ni25Ti10 metallic glass, Intermetallics 16 (2008) 10–15.

[36] S. Lan, Z. Wu, X.-L. Wang, Multiscale structures and phase transitions in metallic glasses: a scattering perspective, Chin. Phys. B 26 (2017) 017104.
[37] X. Sun, G. Mo, L.Z. Zhao, L.H. Dai, Z.H. Wu, M.Q. Jiang, Characterization of nanoscale structural heterogeneity in an amorphous alloy by synchrotron small angle X-ray scattering, Acta Phys. Sin. 66 (2017) 176109.
[38] J.S. Harmon, M.D. Demetriou, W.L. Johnson, K. Samwer, Anelastic to plastic transition in metallic glass-forming liquids, Phys. Rev. Lett. 99 (2007) 135502.
[39] Z.H. Li, Z.H. Wu, G. Mo, X.Q. Xing, P. Liu, A small-angle X-ray scattering station at Beijing synchrotron radiation facility, Instrum. Sci. Technol. 42 (2014) 128–141.
[40] Y. Huang, J.C. Khong, T. Connolley, J. Mi, The onset of plasticity of a Zr-based bulk metallic glass, Int. J. Plast. 60 (2014) 87–100.
[41] S.P. Pan, J.Y. Qin, W.M. Wang, T.K. Gu, Origin of splitting of the second peak in the pair-distribution function for metallic glasses, Phys. Rev. B 84 (2011) 092201.
[42] M. Stoica, J. Das, J. Bednarcik, H. Franz, N. Mattern, W.H. Wang, J. Eckert, Strain distribution in Zr 64.13 Cu 15.75 Ni 10.12 Al 10 bulk metallic glass investigated by in situ tensile tests under synchrotron radiation, J. Appl. Phys. 104 (2008) 013522.
[43] T. Nasu, M. Sasaki, T. Usuki, M. Sekine, Y. Takigawa, K. Higashi, S. Kohara, M. Sakurai, Z. Wei, A. Inoue, Direct observation of radial distribution change during tensile deformation of metallic glass by high energy X-ray diffraction method, J. Alloy. Comp. 483 (2009) 589–592.
[44] K.E. Jensen, D.A. Weitz, F. Spaepen, Local shear transformations in deformed and quiescent hard-sphere colloidal glasses, Phys. Rev. E 90 (2014) 042305.
[45] M. Zink, K. Samwer, W.L. Johnson, S.G. Mayr, Plastic deformation of metallic glasses: size of shear transformation zones from molecular dynamics simulations, Phys. Rev. B 73 (2006) 172203.
[46] D. Pan, A. Inoue, T. Sakurai, M.W. Chen, Experimental characterization of shear transformation zones for plastic flow of bulk metallic glasses, PNAS 105 (2008) 14769–14772.
[47] Y. Fan, T. Iwashita, T. Egami, How thermally activated deformation starts in metallic glass, Nat. Commun. 5 (2014) 5083.
[48] Y. Shao, K. Yao, M. Li, X. Liu, Two-zone heterogeneous structure within shear bands of a bulk metallic glass, Appl. Phys. Lett. 103 (2013) 171901.
[49] A. Guimer, G. Fournet, Small Angle Scattering of X-Rays, J. Wiley & Sons, New York, 1955.
[50] Y.H. Liu, G. Wang, R.J. Wang, D.Q. Zhao, M.X. Pan, W.H. Wang, Super plastic bulk metallic glasses at room temperature, Science 315 (2007) 1385–1388.
[51] Y.H. Liu, D. Wang, K. Nakajima, W. Zhang, A. Hirata, T. Nishi, A. Inoue, M.W. Chen, Characterization of nanoscale mechanical heterogeneity in a metallic glass by dynamic force microscopy, Phys. Rev. Lett. 106 (2011) 125504.
[52] J.C. Ye, J. Lu, C.T. Liu, Q. Wang, Y. Yang, Atomistic free-volume zones and inelastic deformation of metallic glasses, Nat. Mater. 9 (2011) 619–623.
[53] P.S. Steif, F. Spaepen, J.W. Hutchinson, Strain localization in amorphous metals, Acta Metall. 30 (1982) 447–455.
[54] R. Huang, Z. Suo, J.H. Prevost, W.D. Nix, Inhomogeneous deformation in metallic glasses, J. Mech. Phys. Solid. 50 (2002) 1011–1027.
[55] M.Q. Jiang, W.H. Wang, L.H. Dai, Prediction of shear-band thickness in metallic glass, Scripta Mater. 60 (2009) 1004–1007.